frontiers | Frontiers in Astronomy and Space Sciences

TYPE Original Research
PUBLISHED 09 March 2023
DOI 10.3389/fspas.2023.1016345

OPEN ACCESS

EDITED BY
Konstantinos Dialynas,
Academy of Athens, Greece

REVIEWED BY
Quentin Nénon,
UMR5277 Institut de recherche en astrophysique et planétologie (IRAP), France
Qianli Ma,
Boston University, United States

*CORRESPONDENCE
G. Clark,
george.clark@jhuapl.edu

SPECIALTY SECTION
This article was submitted to Planetary Science,
a section of the journal
Frontiers in Astronomy and Space Sciences

RECEIVED 10 August 2022
ACCEPTED 06 January 2023
PUBLISHED 09 March 2023

CITATION
Clark G, Szalay JR, Sulaiman AH, Saur J, Kollmann P, Mauk BH, Paranicas C, Hue V, Greathouse T, Allegrini F, Glocer A, Garcia-Sage K and Bolton S (2023), Energetic proton acceleration by EMIC waves in Io's footprint tail.
Front. Astron. Space Sci. 10:1016345.
doi: 10.3389/fspas.2023.1016345

Energetic proton acceleration by EMIC waves in Io's footprint tail

G. Clark[1]*, J. R. Szalay[2], A. H. Sulaiman[3], J. Saur[4], P. Kollmann[1], B. H. Mauk[1], C. Paranicas[1], V. Hue[5], T. Greathouse[5], F. Allegrini[5,6], A. Glocer[7], K. Garcia-Sage[7] and S. Bolton[5]

[1]Johns Hopkins University Applied Physics Laboratory, Laurel, MD, United States, [2]Department of Astrophysical Sciences, Princeton University, Princeton, NJ, United States, [3]School of Physics and Astronomy, University of Minnesota, Minneapolis, MN, United States, [4]University of Cologne, Cologne, Germany, [5]Southwest Research Institute, San Antonio, TX, United States, [6]University of Texas at San Antonio, San Antonio, TX, United States, [7]NASA Goddard Space Flight Center, Greenbelt, MD, United States

In this study, we present a survey of energetic proton observations associated with Io's footprint tail (FPT) and compare their signatures with *in situ* measurements of the plasma waves and lower-energy electron environments. We find further supporting evidence that proton acceleration in Io's FPT is likely a consequence of wave–particle interactions *via* electromagnetic ion cyclotron waves that are generated by precipitating electrons into Jupiter's ionosphere. This idea was originally proposed by Clark et al. (2020) and Sulaiman et al. (2020) based on NASA's Juno mission likely transiting Io's Main Alfvén Wing (MAW) during its twelfth orbit (i.e., PJ12). Additionally, the analysis of > 50 keV protons presented here highlights important observational details about the Io–Jupiter interaction as follows: 1) proton acceleration in Io's FPT is a persistent feature and the energy flux carried by the protons is highest at smaller Io-Alfvén tail distances; 2) energetic protons exhibit positive correlations with both plasma waves and <100 keV/Q electrons; 3) during a small number of Io FPT crossings, the protons display finer spatial/temporal structure reminiscent of the electron observations reported by Szalay et al. (2018); and 4) the proton pitch angle distributions are characterized by two types: conic distributions in or near Io's MAW and isotropic elsewhere.

KEYWORDS

space physics, Jupiter, ion conics, auroral (particle) acceleration, Juno

Highlights

- Protons are routinely observed to be accelerated in Io's footprint tail.
- Io's Main Alfvén Wing produces the most energetic outflowing protons to date, with their energy flux highest at smaller Io-Alfvén tail distances.
- Correlation analyses to plasma waves and <100 keV/Q electrons further support the idea that EMIC waves are the likely generator.

Introduction

Io is constantly overtaken by the magnetospheric plasma tied to Jupiter's fast-rotating magnetic field. In this sense, Io acts as an obstacle perturbing the local plasma and magnetic field environment, which gives rise to two types of physical interactions: local and far-field (e.g., Saur et al., 2004a). The far-field interaction—which is the main focus of this study, begins several Io radii away, and involves the Alfvén wings, the auroral footprint, and tail—was established from decades of remote observations across various wavelengths, such as radio (Bigg

et al., 1964; Queinnec and Zarka, 1998; Zarka 2000), infrared (Connerney et al., 1993), and ultraviolet wavelengths (Clarke et al., 1996; Prangé et al., 1996; Gérard et al., 2006; Bonfond et al., 2008; Bonfond et al., 2013; Hue et al., 2019). Alfvén waves develop from the sub-Alfvénic interaction between Io and Jupiter's magnetospheric plasma. In the Io rest frame, standing Alfvén waves develop, which are referred to as Alfvén wings (Goertz et al., 1980; Neubauer 1980). Furthermore, they propagate parallel and antiparallel to the local magnetic field in the rest frame of Jupiter and to the higher latitudes. As the waves travel along Jupiter's magnetic field, they partially reflect at plasma density gradients, for example, the Io plasma torus boundary and Jupiter's ionosphere, and nonlinearly interact with itself, producing a turbulent cascade toward smaller spatial and temporal scales. When the properties of the wave reach kinetic scales associated with the plasma (i.e., the inertial length scale, gyroradius, and gyrofrequency), the wave–particle interactions become important and can further accelerate the plasma. A detailed review of moon–magnetosphere interactions and their local space environments can be found in Saur (2021) and Bagenal and Vincent (2020), respectively.

On 1 April 2018 [i.e., perijove (PJ) 12], the Juno spacecraft passed through or very near Io's Main Alfvén Wing (MAW). One notable surprise from that encounter was the observation of energetic protons being accelerated up to 100 s of keV away from Jupiter (Clark et al., 2020). Simultaneous measurements of the plasma electrons (Szalay et al., 2020a), waves (Sulaiman et al., 2020), and magnetic field (Gershman et al., 2019) suggested that the mechanism accelerating the protons was a cyclotron resonant interaction *via* electromagnetic ion cyclotron (EMIC) waves. Sulaiman et al. (2020) derived a heating rate of ~500 eV s^{-1} based on the electric field spectral densities near the proton cyclotron frequency (f_{pe}), and Clark et al. (2020) concluded it was sufficient to heat protons to the observed characteristic energies of a couple of hundred keV. The generation of EMIC waves was assumed to be the precipitating electrons into the ionosphere (e.g., Strangeway et al., 2005), where some fraction of their energy flux gets converted into plasma wave energy flux. This event underscored the importance of energetic proton acceleration associated with Io's far-field interaction region. However, whether this is a characteristic feature or a function of being near or within the MAW was unknown.

In addition to the case study of PJ12, NASA's Juno mission (Bolton et al., 2017) provides critical measurements of the *in situ* field and particle environment associated with the broader Io footprint tail (Io FPT). In general, we are learning that <100 keV electrons in the high latitude and low Jovian altitude tail region of Io are bidirectional with broadband energy distributions. This is believed to be consistent with stochastic acceleration *via* Alfvén waves (Saur et al., 2018; Szalay et al., 2018; Damiano et al., 2019). Further evidence for and characteristics of Alfvén waves along Io's tail was captured by observations of low-frequency transverse fluctuations in the magnetic field data (Gershman et al., 2019), and dispersionless plasma waves below the proton cyclotron frequency were found by the plasma waves instrument (Sulaiman et al., 2020). A recent survey of the plasma electrons found that the measured energy fluxes are best organized by the so-called "Io-Alfvén tail distance" with an e-folding distance of ~21° (Szalay et al., 2020a). Additionally, multiple populations of low-energy (less than a few keV) protons were observed to be accelerated associated with Io's FPT, both near Jupiter and at the boundary of the Io plasma torus (Szalay et al., 2020b). What is currently absent from the literature is a more comprehensive survey of the energetic ion signatures associated with Io's FPT to make direct comparisons with the precipitating electrons driving the auroral emissions and sourcing plasma waves.

In the present study, we report on energetic proton signatures associated with Io's FPT amassed over Juno's prime mission (i.e., 34 orbits) that cover a broad range of altitudes and longitudes. We focus on measurements made with the Jupiter Energetic Particle Detector Instrument (JEDI) (Mauk et al., 2017a) and make comparisons to the published electron measurements from the Jovian Auroral Distribution Experiment (JADE) (McComas et al., 2017), plasma wave investigation (Kurth et al., 2017), and remote observations from the Ultraviolet Spectrograph (UVS) (Gladstone et al., 2017). This work aims to close the gap in our knowledge regarding charged particle observations contained in Io's far-field region, which was identified to be observationally and theoretically the least understood part of the Io–Jupiter interaction (Saur, 2021).

Io footprint tail observations

Jupiter energetic particle detector instrument data

Observations presented here focus on measurements from Juno/JEDI (Mauk et al., 2017a). JEDI is an energetic particle instrument suite composed of three nearly identical sensors. Two of the sensors, namely, JEDI 90 and JEDI 270, are arranged on the spacecraft deck with their fields of view (FoVs) in the spin plane of the spacecraft. This orientation is optimized for obtaining full pitch angle distributions on short cadences (~1.25 s). One sensor, JEDI 180, has its FoV tilted such that it scans perpendicular to the spin plane and covers the full sky after one spacecraft rotation. Juno rotates at two revolutions per minute (rpm).

Each JEDI sensor is composed of six look directions capable of measuring electrons from ~30 keV to ~1 MeV, protons from ~10 keV to several MeV, and heavy ions from >100 s of keV to ~10 s of MeV. The ion measurements utilize a multiple coincidence system that combines a time-of-flight (TOF) measurement with a total energy measurement from a solid-state detector (SSD). The combination of these two measurements is commonly referred to as a "TOFxE" measurement. The advantage of the additional coincidences is that it greatly reduces noise from background sources such as penetrating particles. This is of particular importance for this study because Io is embedded in Jupiter's harsh radiation environment. In contrast, the JEDI electron measurements are prone to the background because they require an SSD-only measurement. This makes their interpretations more difficult in a high-radiation environment. However, Paranicas et al. (2019) showed that large depletions in the energetic electron fluxes are associated with Io and its wave environment. We focus on TOFxE proton measurements in this study. Pitch angle distributions are obtained by combining the JEDI measurements with the Juno magnetometer (MAG) (Connerney et al., 2017b) measurements of the local magnetic field.

The duration of the Io FPT crossings is relatively short compared to Juno's time spent in other regions of Jupiter's polar and equatorial magnetosphere. The primary reasons are as follows: 1) the interaction region is narrowly confined in latitude due to Io's size and the converging magnetic field geometry and 2) Juno has a large relative

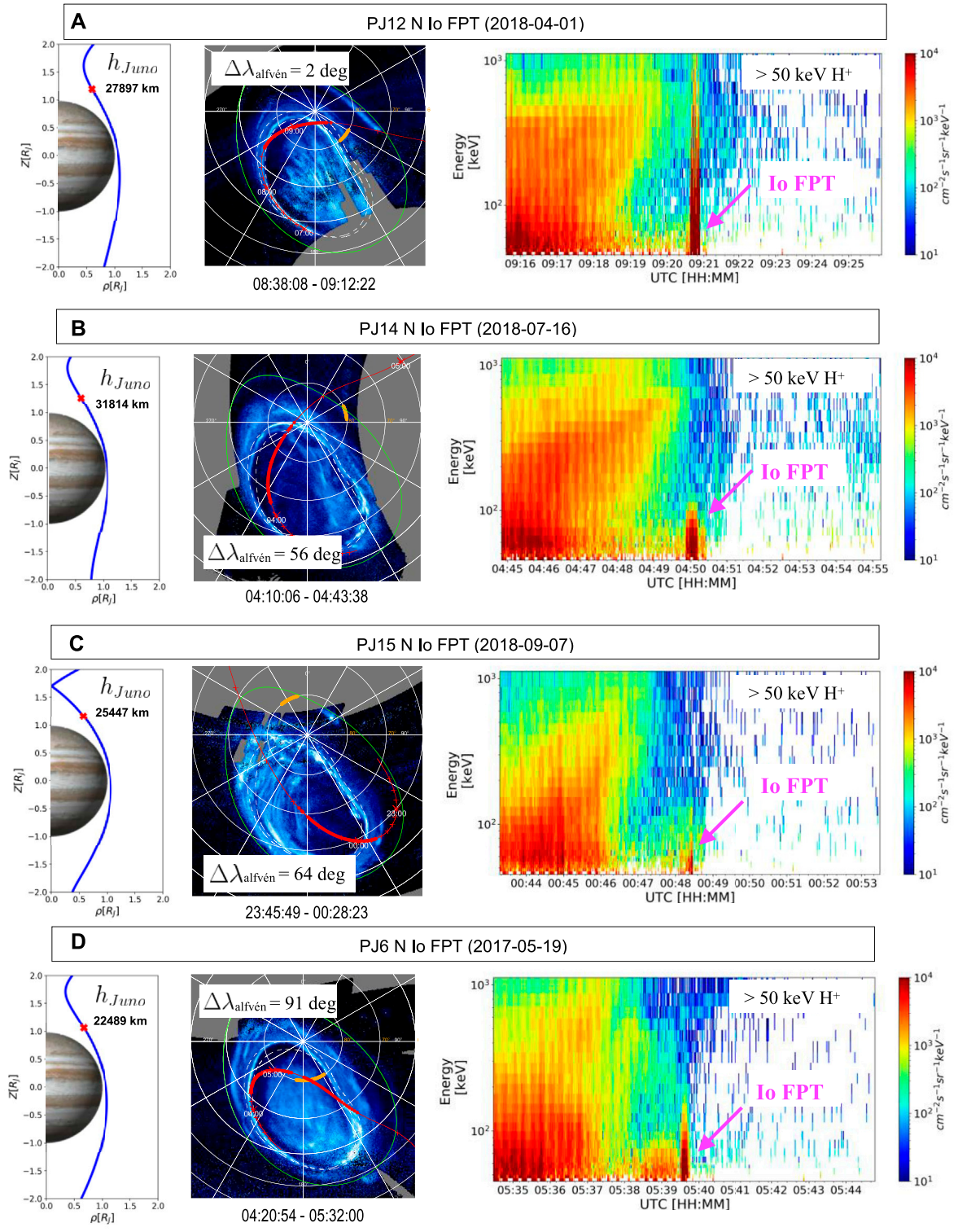

FIGURE 1
Proton signatures associated with the crossing of Io's FPT in Jupiter's northern hemisphere. Panels **(A–D)** are configured the same, where the leftmost panel depicts the trajectory of the Juno spacecraft near perijove (blue curve) in a magnetic cylindrical coordinate system. The red cross mark in the left panel denotes the location and altitude where Juno crosses the FPT. The middle panel is auroral images provided by the Juno UVS instrument. Of those, the red trace corresponds to Juno's footprint track mapped to 400 km above 1 bar using the JRM09 magnetic field model (Connerney et al., 2018). In addition, the green and orange traces map out Io's footprint and the Sun's local time position, respectively. Finally, the last panel shows the energy-time spectrogram of the >50 keV protons where the colors are coded to intensities. The feature corresponding to Io's FPT is highlighted by the magenta arrow.

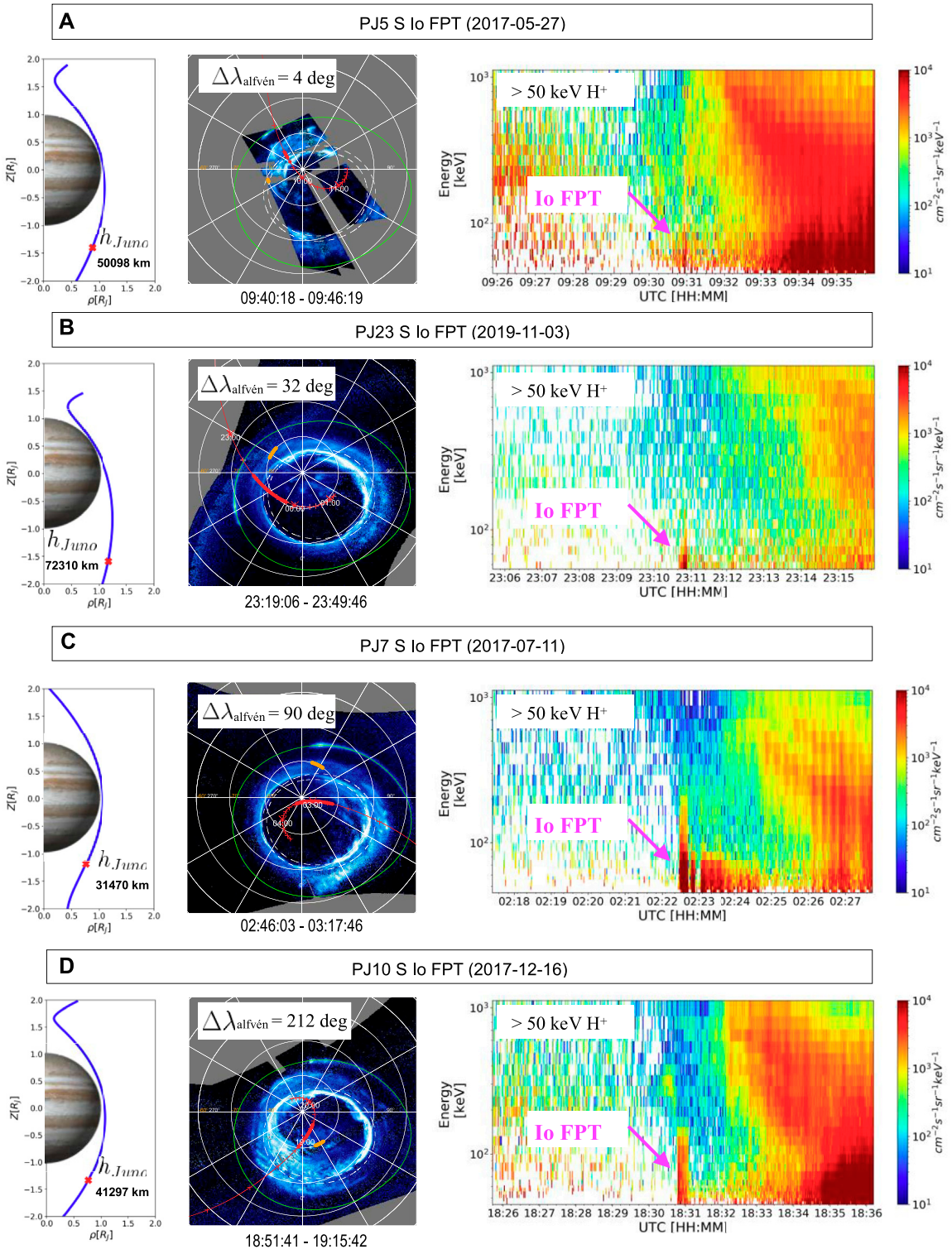

FIGURE 2
The same format as Figure 1, but **(A–D)** represent crossings over Jupiter's southern hemisphere.

orbital velocity, upwards of 40 km s^{-1} through this region. A typical crossing duration lasts approximately 30 s—at the low Jovian altitudes—but can be as short as ~16 s and as long as 60–90 s. To strike a balance between minimizing data sparseness while not averaging out temporal/spatial features, we choose time-averaging windows carefully and dynamically. Some tail crossings support time averaging of the particle intensities as short as 1 s, but other crossings require 2–4 s averaging windows. For the purposes of this study, there is no loss of information by dynamically changing time-averaging windows from event to event; however, it is important to note that all

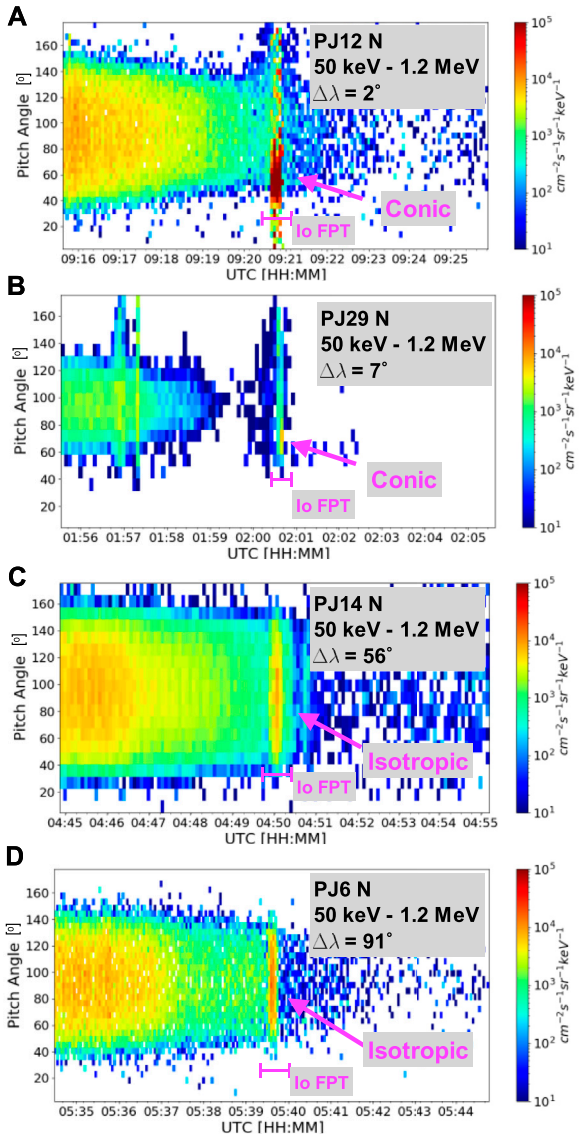

FIGURE 3
Pitch angle distributions for four selected perijoves in the northern hemisphere: PJ12 **(A)**, PJ29 **(B)**, PJ14 **(C)**, and PJ6 **(D)**. Proton PAD for PJ12 and PJ29 illustrates the canonical conic distribution, whereas PJs 6 and 14 indicate isotropic distributions. Note that there are variations in intensity at intermediate pitch angles. The magenta horizontal bar depicts the approximate time range of Juno crossing the Io FPT. Pitch angle distributions are averaged over the energy range of 50 keV–1.2 MeV.

higher order moments (e.g., energy flux and number flux) are calculated using 2 s particle intensity averages.

Representative energetic proton energy-time signatures

InFigures 1, 2, we illustrate a subset of events representative of the proton signatures associated with Io's tail crossings in the north (Figure 1) and south (Figure 2). Plots containing the pitch angle- and energy-time spectrograms of all low-altitude FPT crossings can be found in the Supplementary Materials. Both figures are configured similarly, where each panel contains the trajectory of Juno (blue curve) in cylindrical magnetic coordinates, where the red cross depicts the location and altitude of Juno when it crossed the Io FPT; auroral emissions are observed by Juno UVS (Gladstone et al., 2017) (note the emissions are not simultaneous but rather provide contextual information) and a >50 keV proton energy-time spectrogram highlighting the characteristics of the ions during that crossing. In each figure, the panels are arranged such that the smallest angular separation between Juno's footprint and the initial Alfvén wave (using the Szalay et al., 2020a formulism) is on the top and increases in subsequent panels. In Figure 1A, the PJ12 crossing was the most intense to date in terms of maximum energy and intensity achieved by the protons. This particular event was studied thoroughly from a multi-instrument perspective *via* a series of studies (Clark et al., 2020; Sulaiman et al., 2020; Szalay et al., 2020a) and is believed to be connected to Io's MAW. The remaining panels suggest that proton acceleration is prevalent and even observed at $\Delta\lambda_{\text{Alfvén}}$ separations > 180°. The proton intensity and energy characteristics appear to be related to the increasing $\Delta\lambda_{\text{Alfvén}}$ tail distance. Note that the crossings shown in Figure 1 are all within an altitude range of 3.2×10^4 km (or <0.45 R_J). Therefore, the observed differences are likely not due to variations in altitude. In contrast, the Io FPT crossings in the southern hemisphere occur over a broad range of altitudes (i.e., >0.5 R_J), making the longitudinal differences second-order in nature (see Figures 2A,C). Regardless, accelerated protons on field lines that thread the Io FPT are often observed over a broad range of altitudes, longitudes, and in both hemispheres.

Pitch angle distributions and energy spectra

Aside from the significant increase in intensity and large proton energies achieved in PJ12, another significant difference between the PJ12 event and all others (except PJ29N) are the pitch angle distributions (PADs). Clark et al. (2020) found that during the PJ12 case study, the protons were confined near the upward loss cone, thus indicating a conic distribution. However, nearly all subsequent crossings have much broader pitch angle distributions, as shown in Figure 3. Figure 3A is the PJ12N event showing the conic distribution, and Figures 3C,D depict the PJ14N and PJ6N events showing isotropic distributions, respectively. Figure 3B shows a conic distribution, but it is short-lived and not as dramatic as the PJ12N case. PJ6N and PJ14N represent the other northern and southern hemisphere events observed by JEDI. The isotropic distributions indicate quasi-stably trapped protons bouncing between magnetic mirror points. There are at least three possible scenarios that may explain the trapping distributions observed here: 1) remnant auroral processes where significant scattering has taken place; 2) continuous transverse heating via the wave field; 3) magnetospheric populations on Io field lines.

Although we cannot definitively state which scenario is dominant with our current dataset and theoretical understanding, we inspect the JEDI energy spectra and spatial and temporal features to gain further insight.

First, we present the energy spectra for all Io FPT crossings, showing accelerated proton populations in Figure 4. Energy spectra for the northern and southern hemispheres are shown separately in the left and right panels of Figure 4, respectively. Error bars

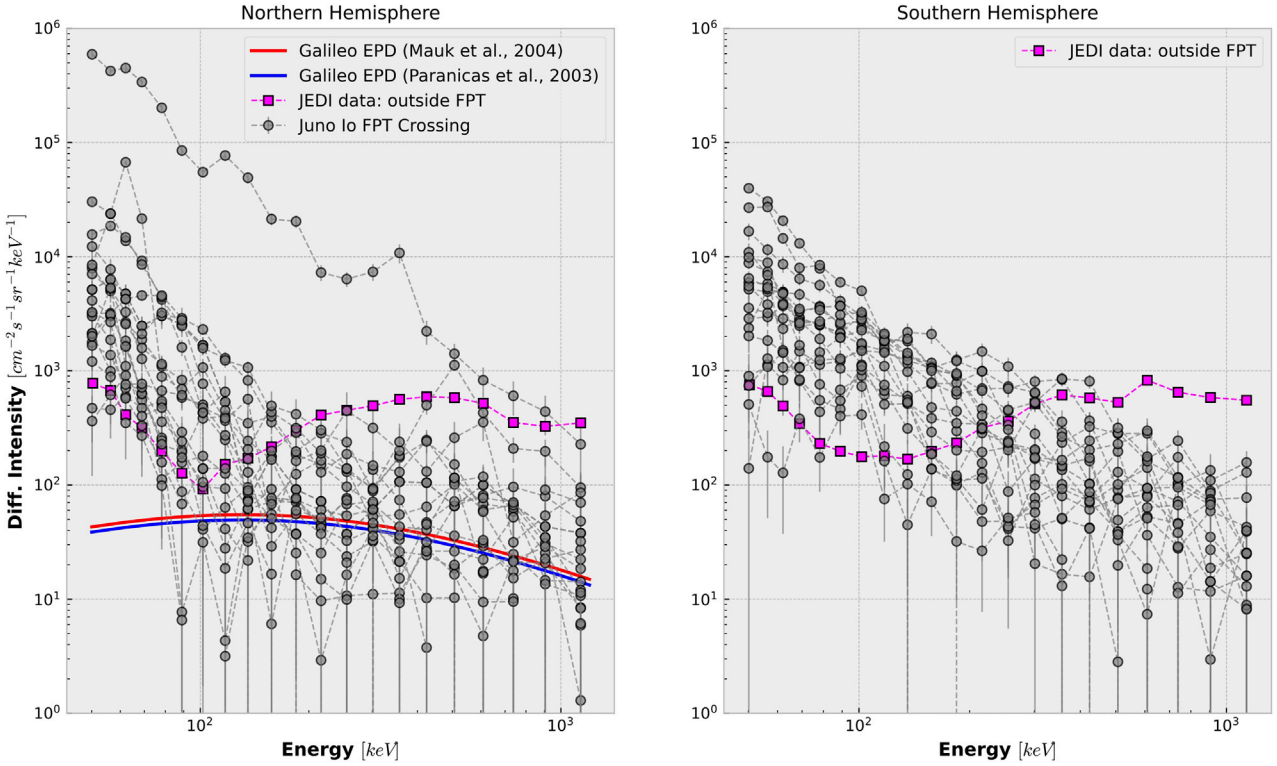

FIGURE 4
Differential H^+ intensity spectra as a function of energy collected by Juno/JEDI during the low-altitude crossings of Io's FPT in both the northern (left panel) and southern (right panel) hemispheres. All spectra were taken from times when the particle energy and number fluxes peaked during the crossing in Supplementary Appendix) and were time averaged over 2 s. Red and blue solid curves represent Galileo EPD measurements near Io in the equator, and the magenta curve depicts JEDI observations of the environment just poleward of Io's FPT (mapping to M-shells of ~7 R_J).

correspond to Poisson counting uncertainties. The two solid line curves represent spectra obtained from the Galileo Energetic Particle Detector (EPD) instrument during an Io flyby near the magnetic equator (unlike the high-latitude, low-altitude footprints obtained by Juno). As noted in Figure 4 plot legend, the red and blue curves are spectral fits, constrained with observations from Paranicas et al. (2003) and Table 1 therein and Mauk et al. (2004) and Table 1 therein, respectively. The energy distributions of protons near the magnetic equator appear to have much lower differential intensities and different spectral shapes compared to the Io FPT proton distributions. The magenta curve with square markers depicts an energy spectrum obtained from Juno just poleward of Io's FPT (on field lines that trace just beyond Io's orbit, i.e., M-Shell ~7 R_J). The spectrum is non-monotonic with a minimum near ~100 keV, which is similar in the northern and southern hemispheres. The <200 keV spectrum is likely sculpted by interactions with the plasma, neutral, and wave environment (Paranicas et al., 2019; Kollmann et al., 2021; Mauk et al., 2022). We include it here to show that the Jovian environment near Io exhibits different qualities based on the trapped populations passing through the neutral gases and plasmas confined near the equator. The roughly 50–100 keV proton intensities associated with nearly all the FPT crossings exhibit larger fluxes than their equatorial counterparts, as observed with EPD, as well as the intensities of the trapped population on field lines just beyond Io. Finally, there appear to be spectral shape differences between the northern and southern FPT crossings. However, note that the altitude ranges are quite different in the two hemispheres due to Juno's trajectory.

Figure 5 shows a comparison of the upgoing energetic protons measured by Juno/JEDI (Figure 5A) to precipitating electrons measured by Juno/JADE (Figure 5B) during the PJ7S Io FPT crossing. The integral energy fluxes are superimposed as white dots (Mauk et al., 2017). Numerical labels 1–3 highlight three general features of both datasets. JADE observations between labels 1 and 2 are decimated partially due to incomplete coverage of pitch angles near 0°. However, this does not negate the finding of fine spatial or temporal structure (Szalay et al., 2018 and Figure 3 therein). In contrast, the pitch angle coverage for JADE between labels 2 and 3 does not change. Although there appears to be general agreement between the two species regarding finer structure, the start times for the lower-energy electrons precede the energetic ions by ~1–2 s. Interestingly, the energetic protons exhibit similar structured spatial and temporal behavior as the lower-energy electrons. We discuss the implications of Figures 3–5 on the three scenarios posed at the beginning of Section 2.3 in Section 3.

Event characterization and magnetic field mapping

To facilitate the statistical analyses that will follow in this section, we characterize the Io FPT events using a crude qualitative assessment

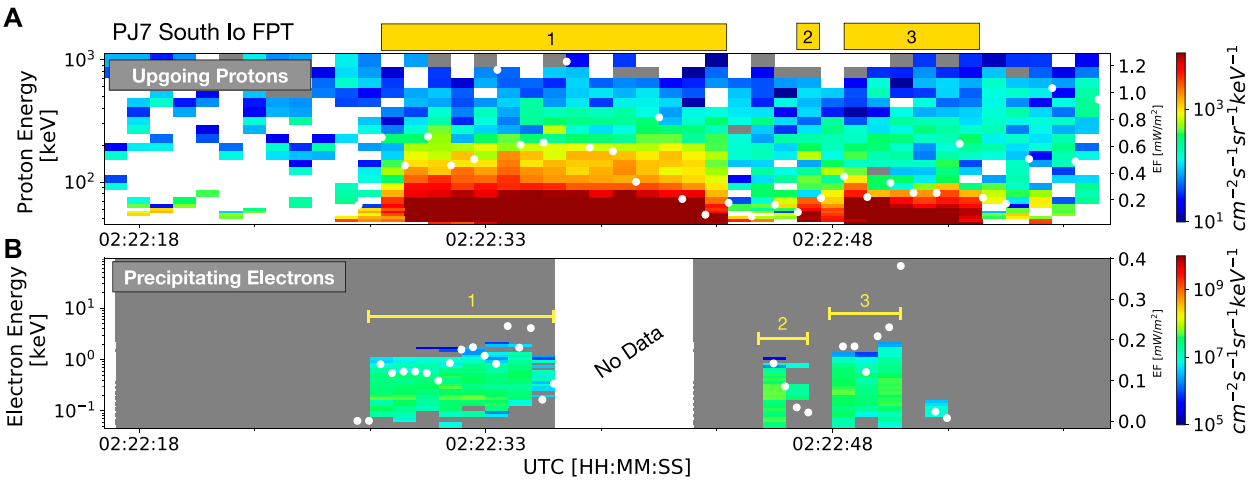

FIGURE 5
PJ7 south split tail structure illustrated by the Juno/JEDI upgoing proton observations averaged over all pitch angles **(A)** and Juno/JADE precipitating electron **(B)** measurements. Superimposed white dots represent integral EF values that correspond to the vertical axis on the right of both panels. Numerical labels identify the three main features interpreted as Io's split tail. White regions correspond to no data, whereas gray regions correspond to zero intensity values.

based on the following criteria: if the H^+ intensities in the ~50–200 keV energy range appear near the predicted time of the FPT crossing and are well separated from the ambient environmental populations with increases ~5–10×, then we denote it has a high-quality event. If we can distinguish an FPT by the H^+ intensities alone, but they are less than a factor of five above adjacent regions, we label it medium quality. If the intensities near the predicted crossing time are indistinguishable, then we discard the event. Figure 6 shows examples of energy-time spectrograms for several crossings and their associated qualitative assessments.

The events are magnetically mapped using the "JupiterMag" tracing code (James, M. K., Wilson, R. J., Vogt, M. F., Provan, G., Kamran, A., Brennan, M. J., & Cowley, S. W. H. JupiterMag [Computer software]) on GitHub, and their M-Shell distributions are displayed in Figure 7. Furthermore, the distributions are separated into their quality classifications, and Io's orbital radii are superimposed as vertical red lines. The events are clustered around Io's orbital position but peak just inside by ~0.15 ± 0.05 R_J. The significance of the peak residing just inward of Io's M-Shell is uncertain. Errors in the magnetic field mapping do exist and may add to this offset, or the peak of the M-Shell distribution could be offset due to the physics could be offset indicative of the physics (e.g., interaction region and Alfvén wave geometry). When separated by high and medium quality, there is an apparent bi-modal shape where the medium-quality events peak near 5.9 R_J. Regardless, the clustering of events analyzed here maps the vicinity of Io and is consistent with the FPT location. A timing analysis is also performed, and the results are included in the Supplementary Appendix.

Io-Alfvén angle and altitude dependencies

A recent survey of the plasma electrons found that the measured energy fluxes are best organized by the so-called "Io-Alfvén tail distance" with an e-folding distance of ~21° (Szalay et al., 2020a). Here, we perform a similar analysis with the energetic H^+ events. Figure 8 shows the Io-Alfvén ($\Delta\lambda_{Alfvén}$) distance (defined in the schematic representation at the top of the plot) and altitude dependence of JEDI proton energy fluxes (Figure 8A) and number fluxes (Figure 8D) associated with Io's FPT. The data points are color coded with altitude information matching the color bar (with some, but not all, PJs specifically labeled), and it can be seen that altitude does not organize the energy and number fluxes. The magenta arrows illustrate FPT crossings that did not result in enhanced H^+ fluxes. Approximately 60% of the crossings—overall $\Delta\lambda_{Alfvén}$—resulted in a positive detection of energetic H^+. Figures 8C,D plot the energy fluxes categorized by their quality classification and the hemisphere of the crossing, respectively. The red dashed curves in Figures 8B,D are best fits of an exponential function (of similar form in Szalay et al., 2020a) to the high-quality crossings. The e-folding angles associated with the fits are 0.57 and 0.35°, respectively. These angles are much smaller than the 21° reported by Szalay et al. (2020a) using the plasma electron observations. It appears that beyond several degrees, the higher-order moments are relatively flat—perhaps a weak dependence on the high-quality data points—for all $\Delta\lambda_{Alfvén}$ distances. The wave ESD power (with correction factors applied, see the following text) exhibits a similar trend as the proton energy fluxes. A similar exponential fit was performed to the wave observations—even though fit does a poorer job at capturing all points—and we find an e-folding angle of 3.2°, suggesting a broader, but somewhat consistent dependence on $\Delta\lambda_{Alfvén}$ distance. In contrast to the flatter response at the larger distances in the H^+ data, the corrected waves' spectral densities show more gradual decreases with increasing distance.

Correlation analysis

In Section 2.3, we suggested three possible scenarios contributing to different PADs. To gain further insight into these scenarios, we

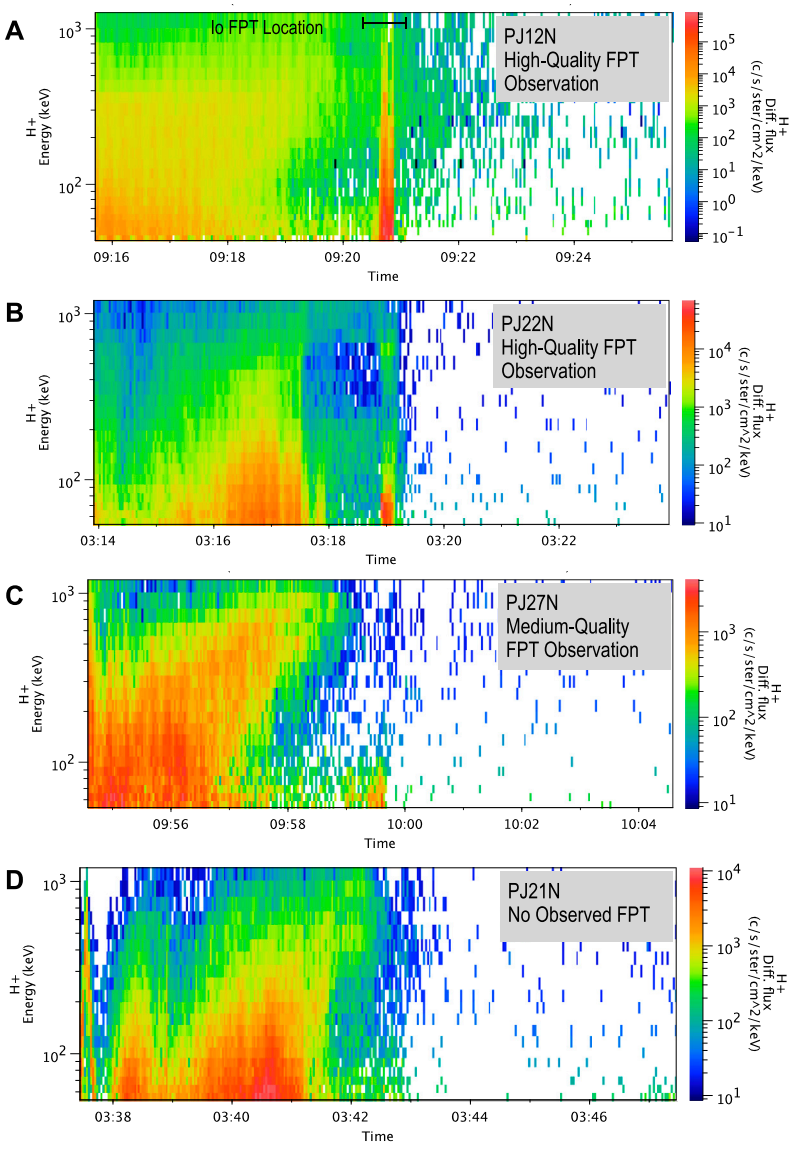

FIGURE 6
Four Io FPT events illustrating our classification scheme. Each panel represents an energy-time spectrogram with color-coded differential intensities. So-called high-quality events are shown in **(A)** and **(B)**, medium-quality in **(C)**, and no identifiable event in **(D)**

examine the correlations between energetic proton populations and the high-frequency wave power, as well as the <100 keV precipitating electron energy fluxes. The wave power was obtained from the Juno Waves investigation (Kurth et al., 2017) and <100 keV electrons from the Juno/JADE electron sensor (McComas et al., 2017). These observables are chosen because they are established from terrestrial observations that strong correlations exist between these parameters (e.g., Strangeway et al., 2005). Figure 9A shows the logarithm of peak energy flux in the >50 keV protons *versus* the logarithm of electric field spectral density (ESD) measured in the proton cyclotron frequency, f_{cH^+}, range $\frac{1}{2}f_{cH^+} < f < f_{cH^+}$. There is also a multiplicative correction factor that accounts for the f_{cH^+} and the angle between the measured electric field and the background magnetic field. We define the correction factor as $\sin(E\angle B)^2 f_{cH^+}$. The angle correction is important because it considers that the wave power depresses parallel to the field and maximizes perpendicular. The peak energy flux in the protons corresponds to the peak within the short time window when Juno crossed the Io FPT. The red and blue dashed lines represent log–log (base 10) regression analyses of all events and those classified as "high-quality," respectively, and similarly defined in the other panels. We also report the correlation coefficients r based on log–log regressions. The PJ12N event is annotated to illustrate the parameters associated with the only likely MAW crossing to date. The correlation between the energetic protons and ion-cyclotron wave power is markedly better when only the high-quality data points (r = 0.58) are considered. However, both fits suggest positive correlations.

Similar regression analyses are displayed for the peak JADE electron energy fluxes *versus* the corrected wave ESD (Figure 9B) and peak JEDI proton energy fluxes *versus* the peak JADE electron energy fluxes (Figure 9C). Correlations between the plasma electrons and waves are investigated to determine if they are ultimately linked to the origin of the observed EMIC waves. Correlations are found

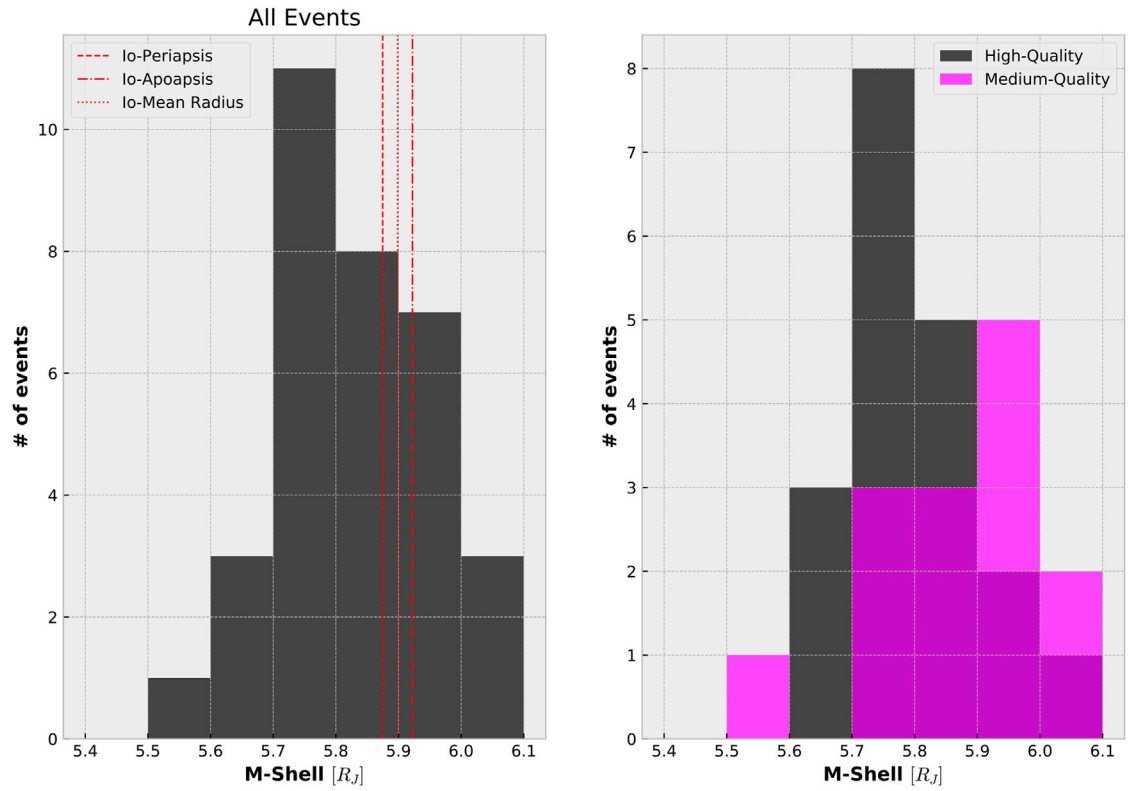

FIGURE 7
M-Shell (in units of Jovian radii) distributions corresponding to all Io FPT events displaying increased H^+ intensities. Orbital information of Io is shown as vertical red lines (left panel), and the histograms separated by event quality are displayed in the right panel. The following arguments were used in the JupiterMag trace field function (see text for citation to GitHub): equation type, "integral"; verbose, "True"; IntModel, "jrm33"; ExtModel, "Con 2020."

between the different datasets and are as follows: $r = 0.98$ (JEDI proton EF *vs*. JADE electron EF) and $r = 0.38$ (JADE electron EF *vs*. corrected wave ESD). These values correspond to only the high-quality events, but the coefficients to all the events are also reported in Figure 9. The Supplementary Appendix includes several Io FPT examples of the frequency-time and energy-time signatures associated with the plasma waves and energetic protons, respectively.

Summary and discussion

Clark et al. (2020) revealed that energetic proton conics are generated in Io's FPT as a result of strong wave heating at altitudes near the auroral region. This event occurred with Juno's PJ12 crossing and was notable because Juno likely crossed Io's MAW, where the Alfvénic interaction is thought to be the strongest. Here, we amassed proton observations from FPT crossings at various distances down tail from over Juno's prime mission and found that energetic proton acceleration signatures are a persistent feature. What is interesting, however, is that the angular distribution of the protons appears to have two different types: conic or isotropic. These contrasting features can be interpreted as manifestations of the same process, originating as proton conics, but scattering broadens the pitch angle profile. To further understand this difference, we looked at the correlations between the peak energy flux in the energetic protons and the peak electric spectral densities in waves, as well as the peak energy flux in the <100 keV electrons. That analysis (see Figure 9) shows modest-to-strong correlations with all three observables. In all cases, the electrons were bi-directional along the local magnetic field and exhibited broadband energy distributions—a feature associated with Alfvénic acceleration (Szalay et al., 2018; Szalay et al., 2020b). The wave power near the proton cyclotron frequency was also enhanced. The concurrence of these features and their positive correlations likely indicate active acceleration below the spacecraft during the crossings. We also investigated alternative scenarios that may produce these signatures; the trapped magnetospheric protons near Io that may resemble outflow. We presented the energy spectra of all the crossings and compared them to the energy spectra obtained by Galileo EPD during an Io flyby and the environmental spectra nearby (in time) obtained by Juno. We found that energy distributions have much higher intensities associated with FPT crossings (see Figure 4). Additionally, the spectra observed by Juno just beyond Io illustrate a very different shape where the low-energy protons are reduced significantly. We interpret this as charge exchange losses in the gas cloud based on studies by Mauk et al. (2022) and Lagg et al. (2003) but do not prove it here. Therefore, it is unlikely that the trapped magnetospheric protons manifest as accelerated outflow signatures. Regardless, we further separated the statistics based on the quality of the events to illustrate that there were no significant changes. Although we cannot prove these distributions originated as conics, thus far, it remains the most reasonable hypothesis.

Szalay et al. (2020a) put forward a new framework called the Io-Alfvén tail distance, which best organized the electron fluxes measured by JADE-E. The authors found that the electron fluxes exponentially diminished with increasing distance from the tail with an e-folding distance of 21°. We adopted that the same framework for organizing

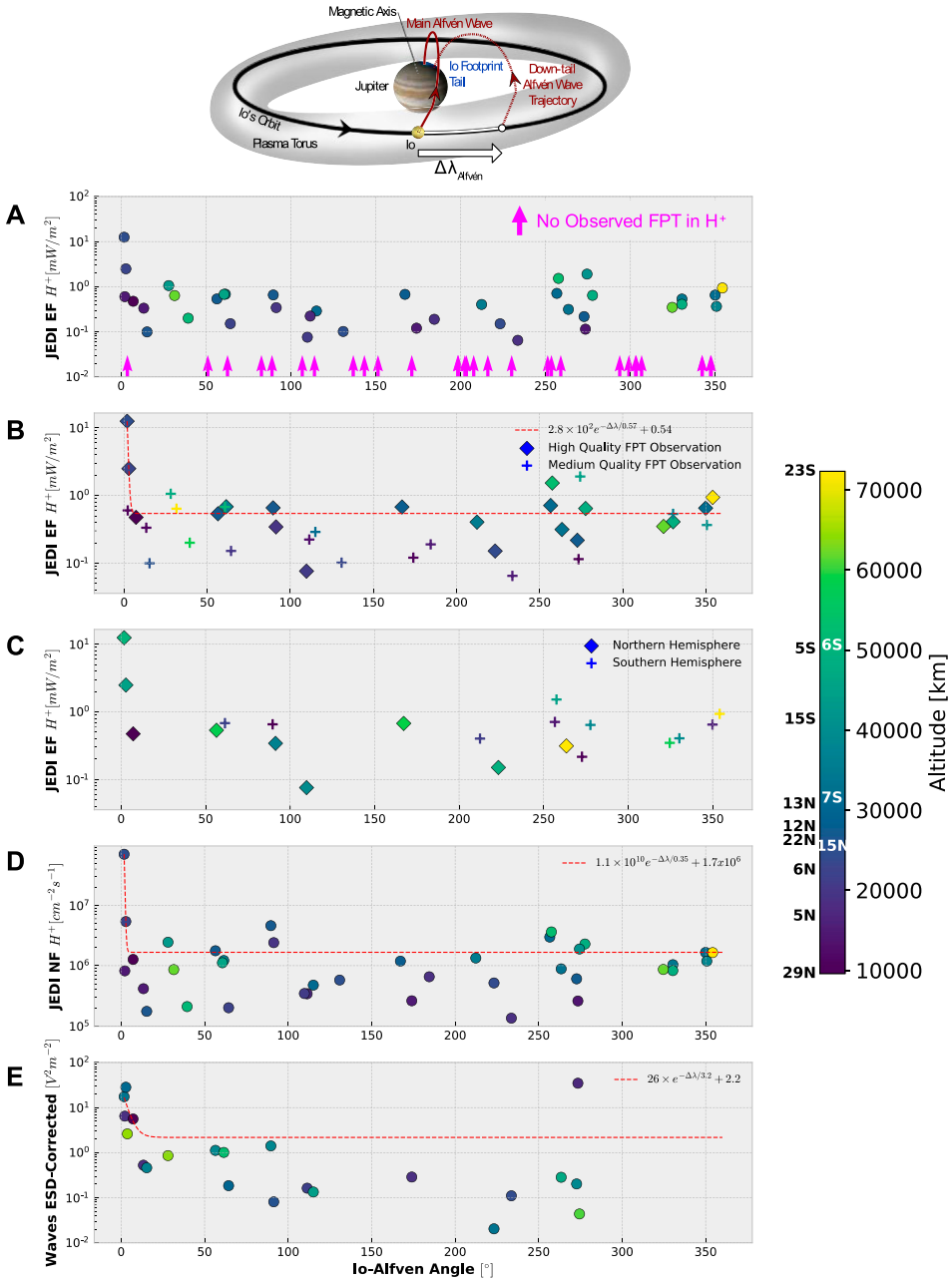

FIGURE 8
JEDI-EF **(A)**, JEDI-NF **(D)**, and wave **(E)** dependence on the Io-Alfvén angle. Markers are color-coded with altitude represented by the color bar and annotated with some of the PJ orbits and corresponding hemispheres. A best-fit exponential fit is shown as a red dashed curve. E-folding angles are reported in the legends. The inset graphic in the top panel illustrates the definition of the Io-Alfvén angle from Szalay et al. (2020a). See text for definitions of "high quality" and "medium quality" events **(B)**.

the JEDI proton energy fluxes and wave peak spectral densities and found that the e-folding distances were much narrower at 0.57° and 3.2°, respectively. The findings and observations in Figure 3, which highlight conic form in or close to the MAW, show where the most intense proton energization occurs. At distances sufficiently far from the MAW ($\Delta\lambda_{Alfvén}$ of just a few degrees), the pitch angle distributions resemble flat, isotropic-like profiles and exhibit similar magnitude energy and number flux moments. Based on this analysis, one may conclude that proton energization is only occurring in or near the MAW. However, the analysis in Section 2 and the previous discussion show positive correlations between the energy flux carried by the >50 keV protons and the amount of power in the waves, as well as the amount of energy flux in the <100 keV/Q electrons. Additionally, the energetic protons and lower-energy electrons reveal a similar finer structure (see split tail feature in Figure 5). It is difficult to imagine how these two different populations resemble similar temporal/spatial structures if they are not coupled. Therefore, it remains a mystery why the proton angular distributions are not conics at larger Io-Alfvén tail distances and their energy fluxes dramatically decrease quickly as a function of down tail distance and remain relatively flat compared to the electrons. Mauk et al. (2022)

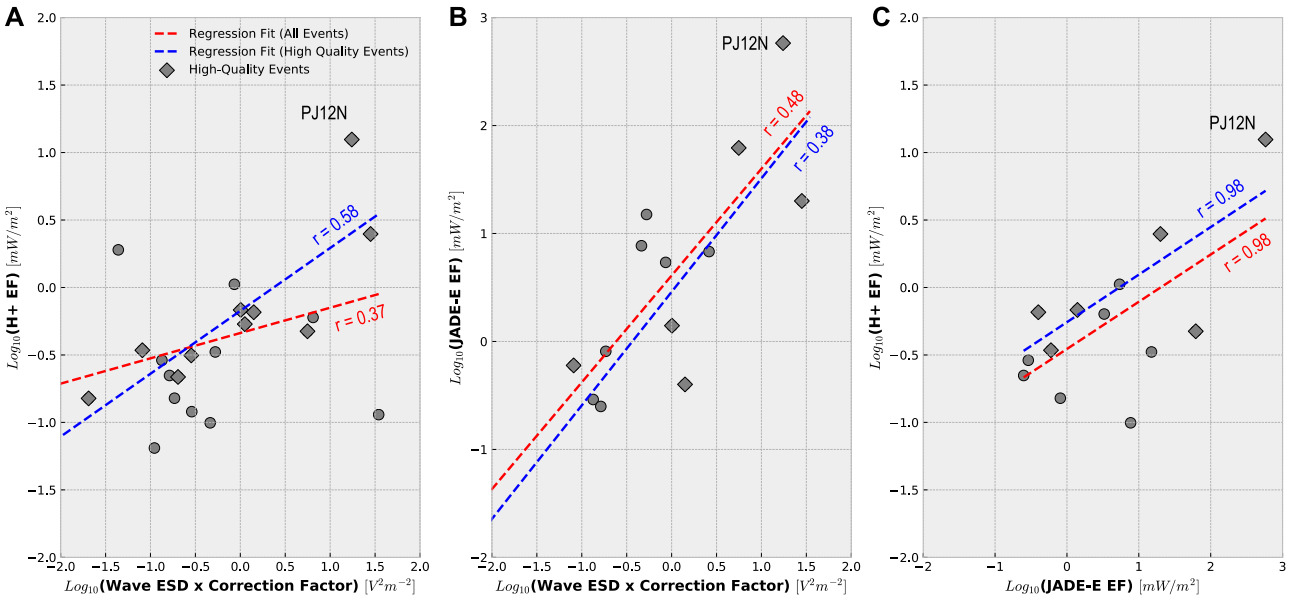

FIGURE 9
Proton energy flux (EF) measurements from Juno/JEDI as a function of Juno/Wave electric field spectral densities (ESD) multiplied by the correction factor discussed in the text **(A)**. Juno/JADE electron EF measurements *vs.* Juno/Waves **(B)** and Juno/JEDI proton EF vs. Juno/JADE electron EF measurements **(C)**. Measurements span various Juno perijove passes. Dashed lines represent regression fits to all events (red) and only high-quality events (blue). Correlation coefficients are reported using the variable *"r."*

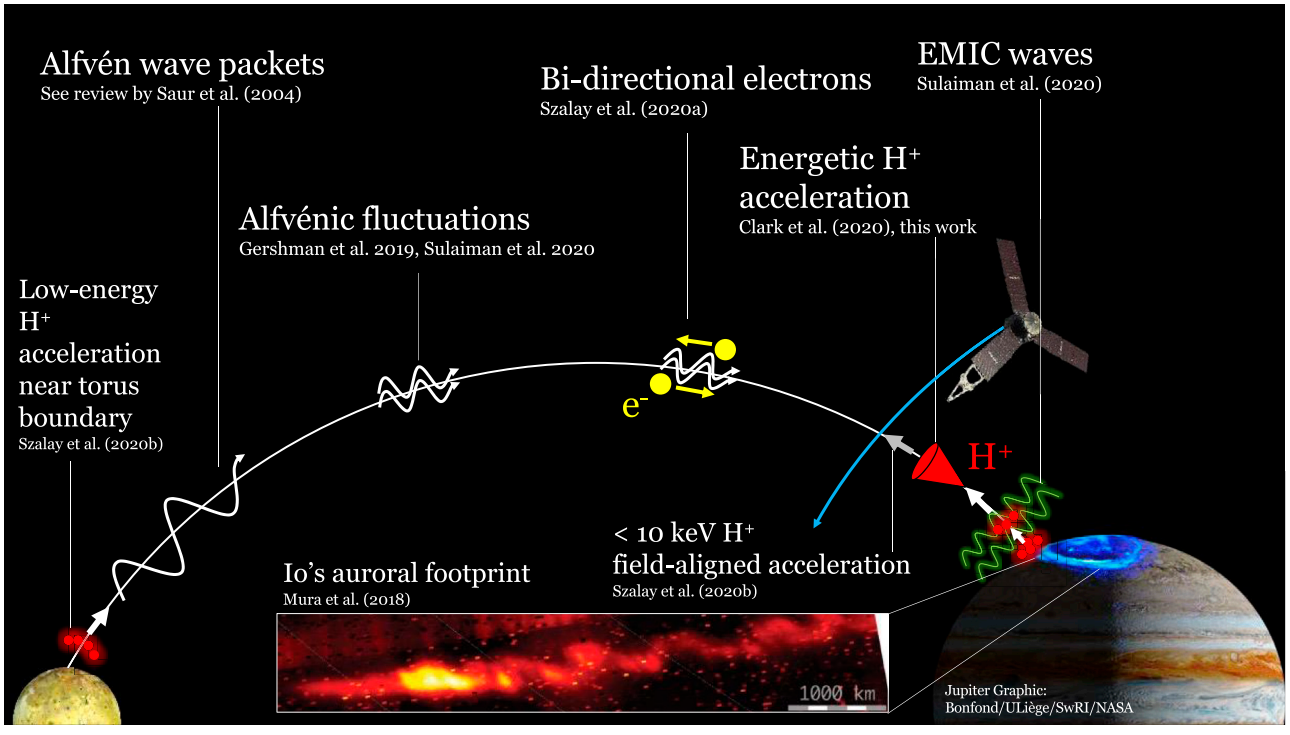

FIGURE 10
Summary graphic of the Io–Jupiter interaction with emphasis on auroral acceleration mechanisms. Main topics are supported with citations. This work focuses on energetic H^+ acceleration as a consequence of the strong Alfvénic interaction between Io and Jupiter. Note: H^+ acceleration does not require the Jovian field lines to be connected directly to Io.

analyzed the loss cone distributions of energetic ions associated with Juno's crossing of the Galilean FPTs and found strong scattering within ~60° of the downstream positions of the moons. Interestingly, Mauk et al. (2022) found a trend on the scattering that resembles, although not as dramatic, the EMIC wave power and energetic proton energy flux trends presented in Figure 8. Therefore, we believe future studies should investigate potential causal links between the high-latitude wave environment and the scattering of the energetic protons to help quantify ring current losses at Jupiter.

Szalay et al. (2020b) showed that low-energy (~0.5–6 keV), field-aligned protons were associated with Io's FPT during Juno's PJ18 pass. Conserving the first adiabatic invariant, the authors determined that the field-aligned protons originated in an altitude range of 0.9–2.5 R_J. How those lower-energy populations are related to the more energetic protons presented here is unclear, but they may be related. For example, that population of protons may be the same population JEDI observes at the higher energies, but for unknown reasons, they were not further energized. Those reasons may include the following: 1) the development of potential low-altitude structures accelerates ions upward to a few keV 2) or perhaps the lower-energy protons originated as conics, but the wave turbulence was far weaker and, therefore, less energy available to protons. The first scenario will produce field-aligned protons due to the nature of parallel acceleration; however, the second scenario requires transport along the field line to regions of weaker magnetic flux to produce more field-aligned distributions. Future studies and modeling efforts should consider the various types of proton distributions associated with Io's FPT as shown here as well as those studied by Szalay et al. (2020b), Clark et al. (2020) to produced a complete theoretical picture of the far-field interactions between Io and Jupiter.

Ion outflow processes at Earth have been extensively studied and remain of high interest because of their role in sourcing the magnetospheric plasma and controlling the dynamics in the down tail region (Moore & Horwitz, 2007; Moore, Fok, Garcia-Sage, 2014). Strangeway et al. (2005) used data acquired by the Fast Auroral Snapshot (FAST) explorer to investigate the factors controlling ionospheric outflows near Earth's cusp. We compared those factors to those presented here and studied by Sulaiman et al. (2020) and Clark et al. (2020) because there are some similarities and differences, which is interesting from a comparative planetary magnetosphere perspective. Strangeway et al. (2005) presented a flowchart (see their Figure 1) that highlights causal, possibly causal, and correlated relationships between energy input and ion outflows. They found strong positive correlations to two possible causal pathways: 1) the generation of very or extremely low frequency (VLF/ELF) waves *via* dissipation of electromagnetic energy flux and 2) the generation of VLF/ELF waves *via* electron precipitation. Possible is emphasized because Strangeway et al. (2005) noted that these processes might be reasonably coupled. They found the following correlations: r = 0.741 between electron precipitation and ELF/VLF waves, r = 0.855 between electron precipitation and proton outflow, and ρ = 0.743 between ELF/VLF waves and outflow. In this study, r = 0.38 between electron precipitation and EMIC waves, r = 0.98 between electron precipitation and proton outflow, and ? = 0.58 between EMIC waves. It is interesting to note that similar to Strangeway et al.'s (2005) study, we find the strongest correlations are also between the pathway that is unlikely causal (i.e., electron precipitation directly energizing the ions).

Furthermore, we found a modest correlation between the coupling of EMIC waves and energetic ions. However, it is worth noting that the correlation was stronger in the Strangeway et al. (2005) study. Regardless, the far-field interaction between Jupiter and Io produces similar physical pathways in generating energetic proton outflow (or conics), as found in Earth's auroral regions.

Based on the expanded analysis of several Io FPT crossings in this study, we found that the original theory presented by Clark et al. (2020) and Sulaiman et al. (2020) remains the most likely hypothesis; that is, ions in Jupiter's ionosphere are accelerated to large energies *via* interactions with EMIC waves. The source of EMIC waves is likely from precipitating, <100 keV/Q, electrons generated *via* Alfvénic fluctuations. Figure 10 shows these details in a summary graphic. However, this study also uncovered new findings associated with the Io FPT, which include the following:

- Energetic proton signatures are a persistent feature of the low-altitude Juno crossings of Io's MAW and FPT.
- The proton signatures vary in energy and intensity, and we found they are organized with the Io-Alfvén angle, as proposed by Szalay et al. (2020b). In contrast to the <100 keV/Q electrons, the energetic protons and plasma wave power falls off more sharply with increasing $\Delta\lambda_{Alfvén}$ distance.
- Energetic protons have positive and statistically significant correlations with plasma wave electric spectral densities near the proton cyclotron frequencies (i.e., $\frac{1}{2}f_{cH^+} < f < f_{cH^+}$) and precipitating electron energy fluxes.
- The pitch angle distributions of the energetic protons come in two types: 1) the conic distribution and 2) an isotropic with empty loss cone distribution. The conic distribution appears to be only present at small $\Delta\lambda_{Alfvén}$ distances.
- Energetic protons also exhibit finer temporal/spatial structure and match well with Io's split tail feature, as inferred by electron observations (Szalay et al., 2018).

Data availability statement

The datasets presented in this study can be found in online repositories. The names of the repository/repositories and accession number(s) can be found at: https://pds-ppi.igpp.ucla.edu/mission/juno/jno/jedi.

Author contributions

GC led the data analysis and writing. JS and AS provided observations and interpretations and assisted in the design of this study. JSaur contributed to the interpretations of the data. VH and TG provided ultraviolet auroral maps. All authors contributed to this manuscript by reading and providing feedback.

Acknowledgments

The authors are thankful to the institutions and personnel that made the Juno mission and the JEDI instrument successful. They are also

grateful to JHU/APL's Lawrence Brown and James Peachy for their roles in developing the core of the data display software. This work was funded by NASA's New Frontiers Program for Juno *via* a subcontract with the Southwest Research Institute in San Antonio, Texas. The data presented here are available from the Planetary Plasma Interactions Node of NASA's Planetary Data System (https://pds-ppi.igpp.ucla.edu/).

Conflict of interest

The authors declare that the research was conducted in the absence of any commercial or financial relationships that could be construed as a potential conflict of interest.

Publisher's note

Supplementary material

The Supplementary Material for this article can be found online at: https://www.frontiersin.org/articles/10.3389/fspas.2023.1016345/full#supplementary-material

References

Bagenal, Fran, and Vincent, Dols (2020). The space environment of Io and Europa. *J. Geophys. Res. Space Phys.* 1255, e2019JA027485. doi:10.1029/2019ja027485

Bolton, S. J., Lunine, J., Stevenson, D., Connerney, J. E. P., Levin, S., Owen, T. C., et al. (2017). The juno mission. *Space Sci. Rev.* 213 (1), 5–37. doi:10.1007/s11214-017-0429-6

Bonfond, B., Grodent, D., Gérard, J.-C., Radioti, A., Saur, J., and Jacobsen, S. (2008). UV Io footprint leading spot: A key feature for understanding the UV Io footprint multiplicity? *Geophys. Res. Lett.* 35, L05107. doi:10.1029/2007GL032418

Bonfond, B., Hess, S., Gérard, J. C., Grodent, D., Radioti, A., Chantry, V., et al. (2013). Evolution of the Io footprint brightness I: Far-UV observations. *Planet. Space Sci.* 88, 64–75. doi:10.1016/j.pss.2013.05.023

Clark, G., Mauk, B. H., Kollmann, P., Szalay, J. R., Sulaiman, A. H., Gershman, D. J., et al. (2020). Energetic proton acceleration associated with Io's footprint tail. *Geophys. Res. Lett.* 47 (24), e2020GL090839. doi:10.1029/2020gl090839

Clarke, J. T., Ballester, G. E., Trauger, J., Evans, R., Connerney, J. E. P., Stapelfeldt, K., et al. (1996). Far-ultraviolet imaging of Jupiter's aurora and the Io "footprint. *Science* 274 (5286), 404. doi:10.1126/science.274.5286.404

Connerney, J. E. P., Baron, R., Satoh, T., and Owen, T. (1993). Images of excited H_3^+ at the foot of the Io flux tube in jupiter's atmosphere. *Science* 262 (5136), 1035. doi:10.1126/science.262.5136.1035

Connerney, J. E. P., Benn, M., Bjarno, J. B., Denver, T., Espley, J., Jorgensen, J. L., et al. (2017b). The juno magnetic field investigation. *Space Sci. Rev.* 213 (1), 39–138. doi:10.1007/s11214-017-0334-z

Connerney, J. E. P., Kotsiaros, S., Oliversen, R. J., Espley, J. R., Jørgensen, J. L., Joergensen, P. S., et al. (2018). A new model of Jupiter's magnetic field from Juno's first nine orbits. *Geophys. Res. Lett.* 45 (6), 2590–2596. doi:10.1002/2018gl077312

Damiano, P. A., Delamere, P. A., Stauffer, B., Ng, C.-S., and Johnson, J. R. (2019). Kinetic simulations of electron acceleration by dispersive scale alfven waves in jupiter's magnetosphere. ´ *Geophys. Res. Lett.* 46, 3043–3051. doi:10.1029/2018gl081219

Gerard, J.-C., Saglam, A., Grodent, D., and Clarke, J. T. (2006). Morphology of the ultraviolet Io footprint emission and its control by Io's location. *J. Geophys.Res.* 111, A04202. doi:10.1029/2005JA011327

Gershman, D. J., Connerney, J. E. P., Kotsiaros, S., DiBraccio, G. A., Martos, Y. M., -Viñas, F. A., et al. (2019). Alfvénic fluctuations associated with Jupiter's auroral emissions. *Geophys. Res. Lett.* 46, 7157–7165. doi:10.1029/2019GL082951

Gladstone, G. R., Persyn, S. C., Eterno, J. S., Walther, B. C., Slater, D. C., Davis, M. W., et al. (2017). The ultraviolet spectrograph on NASA's Juno mission. *Space Sci. Rev.* 213 (1-4), 447–473. doi:10.1007/s11214-014-0040-z

Goertz, C. (1980). Io's interaction with the plasma torus. *J. Geophys. Res.* 85 (A6), 2949–2956. doi:10.1029/JA085iA06p02949

Kollmann, P., Clark, G., Paranicas, C., Mauk, B., Roussos, E., Nénon, Q., et al. (2021). Electron acceleration to MeV energies at jupiter and saturn. *J. Geophys. Res. Space Phys.* 126 (4), 9110–9129. doi:10.1029/2018JA025665

Kurth, W. S., Hospodarsky, G. B., Kirchner, D. L., Mokrzycki, B. T., Averkamp, T. F., Robison, W. T., et al. (2017). The juno waves investigation. *Space Sci. Rev.* 213 (1), 347–392. doi:10.1007/s11214-017-0396-y

Mauk, B. H., Allegrini, F., Bagenal, F., Bolton, S. J., Clark, G., Connerney, J. E. P., et al. (2022). Loss of energetic ions comprising the ring current populations of jupiter's middle and inner magnetosphere. *J. Geophys. Res. Space Phys.* 127 (5), e2022JA030293. doi:10.1029/2022ja030293

Mauk, B. H., Haggerty, D. K., Jaskulek, S. E., Schlemm, C. E., Brown, L. E., Cooper, S. A., et al. (2017a). The jupiter energetic particle detector instrument (JEDI) investigation for the juno mission. *Space Sci. Rev.* 213 (1), 289–346. doi:10.1007/s11214-013-0025-3

Mauk, B. H., Haggerty, D. K., Paranicas, C., Clark, G., Kollmann, P., Rymer, A. M., et al. (2017). Juno observations of energetic charged particles over Jupiter's polar regions: Analysis of monodirectional and bidirectional electron beams. *Geophys. Res. Lett.* 44 (10), 4410–4418. doi:10.1002/2016gl072286

Mauk, B. H., Mitchell, D. G., McEntire, R. W., Paranicas, C. P., Roelof, E. C., Williams, D. J., et al. (2004). Energetic ion characteristics and neutral gas interactions in Jupiter's magnetosphere. *J. Geophys. Res. Space Phys.* 109 (A9), A09S12. doi:10.1029/2003ja010270

McComas, D. J., Alexander, N., Allegrini, F., Bagenal, F., Beebe, C., Clark, G., et al. (2017). The jovian auroral distributions experiment (JADE) on the juno mission to jupiter. *Space Sci. Rev.* 213 (1), 547–643. doi:10.1007/s11214-013-9990-9

Moore, T. E., Fok, M. C., and Garcia-Sage, K. (2014). The ionospheric outflow feedback loop. *J. Atmos. Solar-Terrestrial Phys.* 115, 59–66. doi:10.1016/j.jastp.2014.02.002

Moore, Thomas E., and Horwitz, J. L. (2007). Stellar ablation of planetary atmospheres. *Rev. Geophys.* 45, 3. doi:10.1029/2005rg000194

Neubauer, F. (1980). Nonlinear standing Alfvén wave current system at Io: Theory. *J. Geophys. Res.* 85 (A3), 1171–1178. doi:10.1029/JA085iA03p01171

Paranicas, C., Mauk, B. H., Haggerty, D. K., Clark, G., Kollmann, P., Rymer, A. M., et al. (2019). Io's effect on energetic charged particles as seen in Juno data. *Geophys. Res. Lett.* 46 (23), 13615–13620. doi:10.1029/2019gl085393

Paranicas, C., Mauk, B. H., McEntire, R. W., and Armstrong, T. P. (2003). The radiation environment near Io. *Geophys. Res. Lett.* 30 (18). doi:10.1029/2003gl017682

Prangé, R., Rego, D., Southwood, D., Zarka, P., Miller, S., and Ip, W. (1996). Rapid energy dissipation and variability of the Io–Jupiter electrodynamic circuit. *Nature* 379 (6563), 323–325. doi:10.1038/379323a0

Saur, J., Janser, S., Schreiner, A., Clark, G., Mauk, B. H., Kollmann, P., et al. (2018). Wave-particle interaction of Alfvén waves in Jupiter's magnetosphere: Auroral and magnetospheric particle acceleration. *J. Geophys. Res. Space Phys.* 123, 9560–9573. doi:10.1029/2018JA025948

Saur, J., Neubauer, F. M., Connerney, J. E. P., Zarka, P., and Kivelson, M. G. (2004a). "Plasma interaction of Io with its plasma torus," in *Jupiter: The planet, satellites and magnetosphere.* Editors F. Bagenal, T. Dowling, and W. McKinnon (New York: Cambridge Univ. Press), 537–560.

Saur (2021). *Magnetospheres in the solar system*, 575–593.Joachim. "Overview of moon–magnetosphere interactions

Strangeway, R. J., Ergun, R. E., Su, Y. J., Carlson, C. W., and Elphic, R. C. (2005). Factors controlling ionospheric outflows as observed at intermediate altitudes. *J. Geophys. Res. Space Phys.* 110 (3), A03221. doi:10.1029/2004ja010829

Sulaiman, A. H., Hospodarsky, G. B., Elliott, S. S., Kurth, W. S., Gurnett, D. A., Imai, M., et al. (2020). Wave-particle interactions associated with Io's auroral footprint: Evidence of Alfvén, ion cyclotron, and whistler modes. *Geophys. Res. Lett.* 47, e2020GL088432. doi:10.1029/2020gl088432

Szalay, J. R., Allegrini, F., Bagenal, F., Bolton, S. J., Bonfond, B., Clark, G., et al. (2020a). A new framework to explain changes in Io's footprint tail electron fluxes. *Geophys. Res. Lett.* 47 (18), e2020GL089267. doi:10.1029/2020gl089267

Szalay, J. R., Bagenal, F., Allegrini, F., Bonfond, B., Clark, G., Connerney, J. E. P., et al. (2020b). Proton acceleration by Io's Alfvénic interaction. *J. Geophys. Res. Space Phys.* 125. doi:10.1029/2019JA027314

Szalay, J. R., Bonfond, B., Allegrini, F., Bagenal, F., Bolton, S., Clark, G., et al. (2018). *In situ* observations connected to the Io footprint tail aurora. *J. Geophys. Res. Planets* 123, 3061–3077. doi:10.1029/2018JE005752

Zarka, P. (2000). Radio emissions from the planets and their moons. *Geophys. Monograph-American Geophys. Union* 119, 167–178. doi:10.1029/GM119p0167